ComEX

High-precision automatic optical axis alignment of LED backhaul in lighting surroundings based on object detection

Yuma Nishimura[1, a)]**, Wataru Chujo** [1, b)]**, and Kentaro Kobayashi** [1]

Abstract   Research on high-throughput optical wireless communication (OWC) has been progressing toward sixth generation. As half-power beam width of near-infrared 600 Mbps light emitting diode backhaul (LEDBH) consisting of LED and photodiode is narrow, high-precision optical axis alignment of LEDBH is important. So far, the optical axis was manually aligned using a scope. In this study, object detection using deep learning, YOLOv7, is adapted to automatically align the optical axis. Average precisions of LEDBH detection are evaluated in lighting surroundings while changing the camera exposure time. The optical axis is finely adjusted with object detection and mechanical angle adjustment.
Keywords: optical wireless communication, optical axis alignment, object detection, deep learning, LED backhaul, 6G
Classification: Wireless communication technologies

1. Introduction

Research on high-throughput OWC has been underway as a new carrier band candidate for sixth generation (6G) wireless communications [1]. OWC receivers are classified into cameras using image sensors and photodiode (PD) receivers. Cameras can simultaneously achieve high spatial resolution and wide-angle field of view (FOV). However, the low data rate property of optical camera communication (OCC) poses a high barrier towards 6G.

On the other hand, PD receivers can achieve high data rates. Integration of local 5G and OWC has also been studied using PD receivers [2]. High-throughput OWC using PD receivers is suitable candidate for 6G.

The drawback of high-throughput PD receivers is that they cannot simultaneously satisfy high spatial resolution and wide-angle FOV like cameras. If half-power beam width of the PD receiver is narrowed to suppress interference, optical axis alignment becomes difficult.

So far, the optical axis of high-throughput full-duplex near-infrared (IR) LEDBHs [3] was manually aligned using a scope. In this study, high-precision automatic optical axis alignment is investigated using object detection.

Generally, to automatically align the optical axis of the transceivers, a camera [4] or a quadrant PD array [5] is used. However, the decision based on thresholds of the camera's received pixel value or the output amplitude of the quadrant PD array has difficulty distinguishing between LEDs for communication and those for lighting in surroundings. In lighting surroundings, these methods may capture multiple LEDs and make false decision.

To identify only the LED transmitter in lighting surroundings, correlation localization techniques and object detection techniques using deep learning (DL) have been proposed. Correlation localization techniques use time-series correlation with transmission patterns of communication LED [6]. On the other hand, object detection using DL detects LED transmitters from captured images with a camera. Detection of LED transmitters using convolutional neural networks has been studied for high-throughput OWC using a PD receiver [7]. However, it is limited to simulations. Identification of communication LEDs and lighting LEDs using You Only Look Once (YOLO) has also been studied [8], which experimentally demonstrates the effectiveness of communication LED detection using DL. However, it is limited to low data rate OCC. There are no studies that combine high data rate PD receivers with object detection by DL using camera images.

In this study, optical axis alignment of a near-IR 600 Mbps LEDBH is experimentally demonstrated by detecting LEDBH using object detection and mechanical angle adjustment using a motor. Average precision (AP) of LEDBH based on object detection and throughput after optical axis alignment are evaluated in lighting surroundings.

2. Experimental configuration and procedure for optical axis alignment using object detection

Figure 1 shows experimental configuration and specifications of LEDBH and camera. Two full-duplex near-IR LEDBHs are facing each other at a distance, d, and the throughput is evaluated in both directions. The data rate and throughput of LEDBH are up to 750 Mbps in physical layer and 600 Mbps in layer 2, respectively. So far, the optical
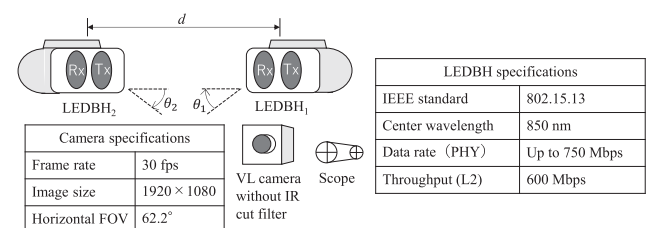
[1] Dept. of Electrical and Electronic Engineering, Meijo University, Tempaku-ku, Nagoya 468-8502, Japan

a) 200442119@ccmailg.meijo-u.ac.jp
b) wchujo@meijo-u.ac.jp

Fig. 1   Experimental configuration and specifications of LEDBH and camera.

axis was manually aligned using a scope. Instead of a scope, a visible light (VL) camera without IR cut filter is attached to the own station, LEDBH$_1$. The camera is 30 frames per second (fps), the image size is full high definition, and the horizontal FOV is 62.2°. The camera detects the opposite station, LEDBH$_2$, and the optical axis is mechanically aligned by a motor so that the offset angle θ_1 of the own station is 0°.

Figure 2 shows the angular characteristics of the throughputs of LEDBH$_1$ evaluated while varying the station's offset angle θ_1 at a distance, $d = 30$ m. The offset angle θ_2 of the opposite station, LEDBH$_2$, is set to 0°. The transmitting angle characteristics are more severe than the receiving. To maintain 600 Mbps, it is necessary to suppress the angle alignment error within ±0.2 degrees.

Figure 3 shows the procedure for automatically aligning the optical axis of LEDBH$_1$. So far, the optical axis was manually aligned using a scope. It is assumed that the approximate location of LEDBH$_2$ is known in advance. First, the offset angle θ_1 of LEDBH$_1$ is coarsely adjusted to within ±1.2° by the motor. Next, the offset angle of LEDBH$_1$ is finely adjusted to 0° by the motor using object detection.

Since LEDs' luminance is generally much higher than the surrounding objects, pixel values captured with the camera are easy to get saturated. Saturation of the pixel values makes it difficult to classify categories with object detection. Therefore, to learn the differences in LED radiation patterns, it is necessary to shorten the camera's exposure time.

Table I shows evaluation parameters to obtain suitable exposure time. In the experiments in subsections 3.1-3.3, it is assumed that the optical axis of the opposite station, LEDBH$_2$ does not align to LEDBH$_1$. AP is evaluated while the offset angle of LEDBH$_2$ is fixed at $\theta_2 = 0.86°$.
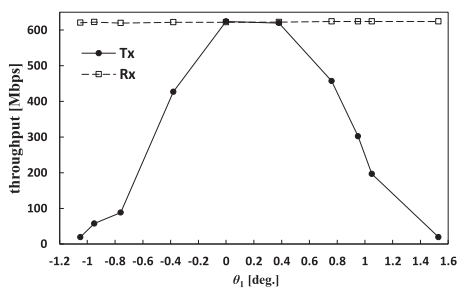

Fig. 2 Throughputs of LEDBH$_1$ versus offset angle, θ_1.
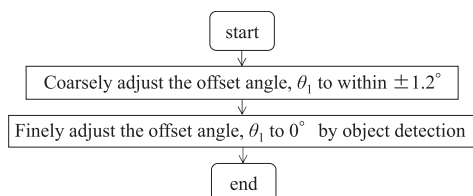

Fig. 3 Procedure for automatically aligning the optical axis.

Table I Evaluation parameters to obtain suitable exposure time.

parameters	surroundings	VL cut	θ_1	θ_2	FOV
subsection 3.1	almost no lighting	no	0°	0.86°	62.2°
subsection 3.2	lots of lighting	no	0°	0.86°	62.2°
subsection 3.3	lots of lighting	yes	0°	0.86°	62.2°

In this study, YOLOv7 is used as the object detection algorithm, where object categories are limited to only one category, LEDBH$_2$. The number of epochs is 400, the ratio of training data, validation data, and test data is 8:2:1, and a total of 440 images are used.

Normally, mean AP (mAP) is used as evaluation metrics for object detection model. However, since LEDBH$_2$ is the only category, AP (IoU (Intersection over Union) ≥ 0.5) is used as the evaluation metrics.

3. LEDBH detection using YOLOv7

3.1 Differences in AP due to exposure time in almost no lighting surroundings

First, differences in AP (IoU ≥ 0.5) due to exposure time was experimentally investigated in almost no lighting surroundings based on the evaluation parameters (see Table I). Figure 4 shows differences in AP using the training data, where the offset angle of LEDBH$_2$ is fixed at $\theta_2 = 0.86°$ and the distance between LEDBH$_1$ and LEDBH$_2$, $d = 10$ m. The number of epochs required for AP convergence increases as the exposure time becomes shorter. These results indicate that the short exposure time is not effective in almost no lighting surroundings. However, compared to 3.2 and 3.3, this is due to insufficient resolution as the LEDBH$_2$ image becomes smaller as the exposure time becomes shorter.

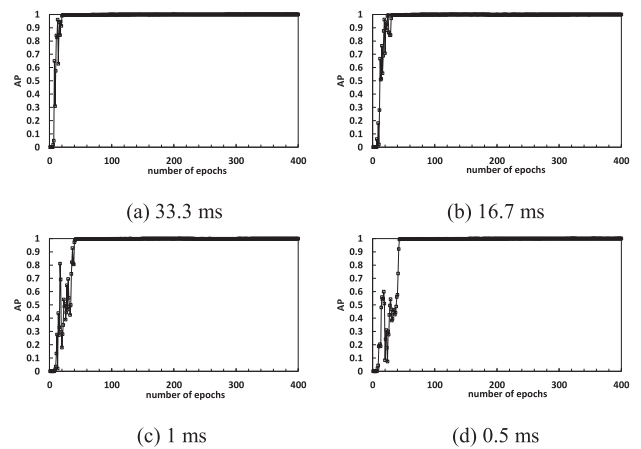In addition, Fig. 5 shows examples of LEDBH$_2$ detection

Fig. 4 Differences in AP (IoU ≧ 0.5) due to exposure time in almost no lighting surroundings ($\theta_2 = 0.86°$, $d = 10$ m).
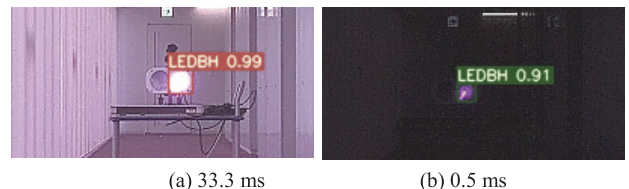

Fig. 5 Examples of LEDBH$_2$ detection in the test data using the trained model in almost no lighting surroundings ($\theta_2 = 0.86°$, $d = 10$ m).

Table II Difference in AP versus exposure time for the test data in almost no lighting surroundings ($\theta_2 = 0.86°$, $d = 10$ m).

exposure time [ms]	33.3	16.7	1	0.5
AP (IoU ≧ 0.5)	1	0.999	0.999	0.999

in the test data using the trained model. Table II also shows the difference in AP versus exposure time for the test data. In Fig. 5, the confidence score decreases slightly as the exposure time becomes shorter. However, in Table II, APs of the test data are above 99.9% regardless of the exposure time. Even when the exposure time is short, confidence score is high in almost no lighting surroundings. However, when the exposure time is short, the effect of improving AP cannot be obtained due to insufficient resolution of LEDBH$_2$.

3.2 Differences in AP due to exposure time in lots of lighting surroundings

Second, differences in AP (IoU $\geq$ 0.5) due to exposure time was experimentally investigated in lots of lighting surroundings based on the evaluation parameters (see Table I). Even when the exposure time is short, if there are lots of lighting in the surrounding area, the effect of improving AP may be obtained. Figure 6 shows differences in AP due to exposure time, where the offset angle of LEDBH$_2$ is fixed at
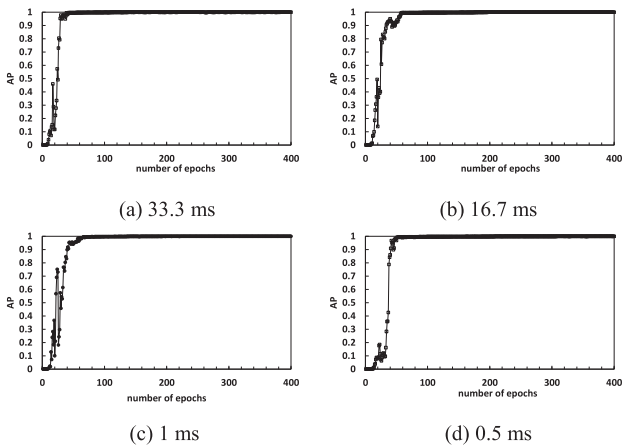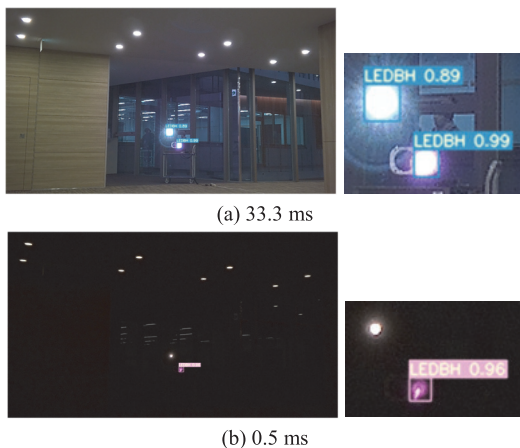
$\theta_2 = 0.86°$ and the distance, $d = 10$ m.

When the exposure times are long, 33.3, 16,7, and 1 ms, the convergence properties of AP in lots of lighting surroundings are worse than those in almost no lighting surroundings (see Figs. 4(a), (b), and (c)). However, when the exposure time is short, 0.5 ms, the convergence property of AP in lots of lighting surroundings is better than that in almost no lighting surroundings (see Fig. 4(d)).

These results indicate that the saturated LEDBH$_2$ and LED lightings images make categories difficult to classify when the exposure times are long. On the contrary, the differences between LEDBH$_2$ and LED lightings radiation patterns can be learned when the exposure time is short.

In addition, Fig. 7 shows examples of LEDBH$_2$ detection in the test data using the trained model. When the exposure time is 33.3 ms in Fig. 7(a), LEDBH$_2$ is detected with a confidence score of 0.99. However, LED lighting is falsely detected with a confidence score of 0.89. On the contrary, when the exposure time is 0.5 ms in Fig. 7(b), only LEDBH$_2$ is correctly detected with a confidence score of 0.96. Moreover, Table III shows the difference in AP versus exposure time for the test data. AP with short exposure time is slightly better than that with long exposure time. These results also indicate that it is easy to learn the differences between LEDBH$_2$ and LED lightings images when the exposure time is short.

3.3 Differences in AP due to exposure time under VL cut condition

Third, differences in AP (IoU $\geq$ 0.5) due to exposure time was experimentally investigated under VL cut condition in lots of lighting surroundings (see Table I). Even where lots of lighting surroundings, only near-IR LEDBH$_2$ can be learned with high resolution using VL cut filter. Figure 8 shows differences in AP due to exposure time under VL cut condition, where the offset angle of LEDBH$_2$ is fixed at $\theta_2 = 0.86°$ and the distance, $d = 10$ m. In lots of lighting surroundings, the convergence properties of AP with VL cut filter is better than those without VL cut filter (see Fig. 6). Moreover, under VL cut condition, the convergence properties of AP when the exposure time is 0.5 ms in Fig. 8(d) is almost the same as those when the exposure time is 33.3 ms
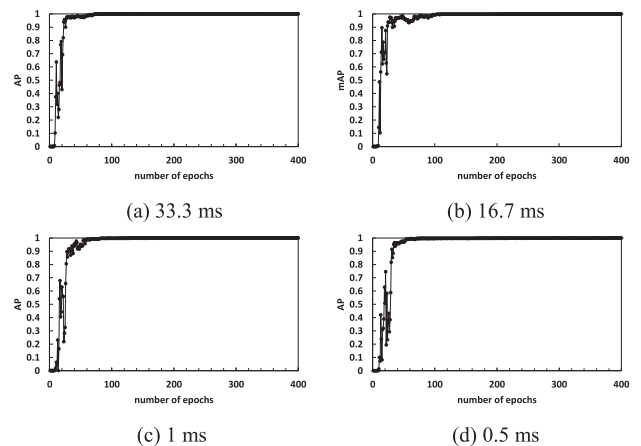

(a) 33.3 ms (b) 16.7 ms

(c) 1 ms (d) 0.5 ms

Fig. 6 Differences in AP (IoU $\geqq$ 0.5) due to exposure time in lots of lighting surroundings ($\theta_2 = 0.86°$, $d = 10$ m).

(a) 33.3 ms

(b) 0.5 ms

Fig. 7 Examples of LEDBH$_2$ detection in the test data using the trained model in lots of lighting surroundings ($\theta_2 = 0.86°$, $d = 10$ m).

Table III Difference in AP versus exposure time for the test data in lots of lighting surroundings ($\theta_2 = 0.86°$, $d = 10$ m).

exposure time [ms]	33.3	16.7	1	0.5
AP (IoU$\geqq$0.5)	0.998	0.998	0.999	0.999

(a) 33.3 ms (b) 16.7 ms

(c) 1 ms (d) 0.5 ms

Fig. 8 Differences in AP (IoU $\geqq$ 0.5) due to exposure time under VL cut condition in lots of lighting surroundings ($\theta_2 = 0.86°$, $d = 10$ m).
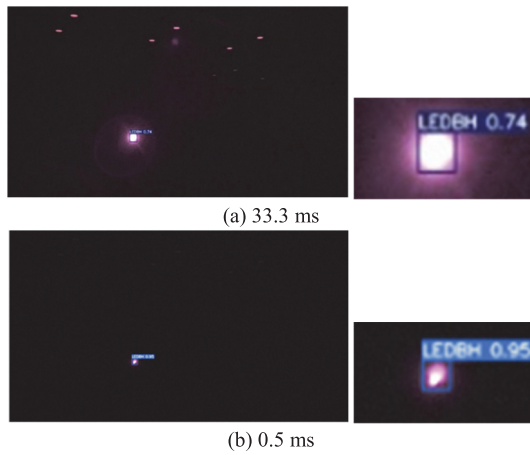
(a) 33.3 ms

(b) 0.5 ms

Fig. 9 Examples of LEDBH2 detection in the test data using the trained model under VL cut condition ($\theta_2 = 0.86°$, $d = 10$ m).

Table IV Difference in AP versus exposure time for the test data under VL cut condition ($\theta_2 = 0.86°$, $d = 10$ m).

| exposure time [ms]	33.3	16.7	1	0.5
AP (IoU$\geqq$0.5)	0.902	0.893	0.997	0.994

in Fig. 8(a). Even when the exposure time is short, LEDBH$_2$ can be learned accurately under VL cut condition.

In addition, Fig. 9 shows examples of LEDBH$_2$ detection in test data using the trained model. When the exposure time is 33.3 ms in Fig. 9(a), confidence score for LEDBH$_2$ decreases to 0.74. On the contrary, when the exposure time is 0.5 ms in Fig. 9(b), confidence score for LEDBH$_2$ increases to 0.95. Table IV also shows the difference in AP versus exposure time for the test data. AP for the test data with short exposure time is much better than that with long exposure time. These results indicate that AP with short exposure time can be improved more than that with long exposure time because the radiation pattern of LEDBH$_2$ can be learned more accurately under VL cut condition.

4. Mechanical optical axis alignment based on object detection

Mechanical optical axis alignment was conducted based on object detection under VL cut condition (see subsection 3.3), where the exposure time is reduced to 34 μs, the offset angle of LEDBH$_2$, $\theta_2 = 0°$, and the distance, $d = 10$ m. After coarse alignment of the offset angle θ_1 of LEDBH$_1$ within ±1.2°, the angle is finely aligned to 0° by the motor using object detection (see Fig. 3). Figure 10(a) shows horizontal single-axis control mechanism for LEDBH$_1$. The angular resolution and accuracy of the motor are 0.1° and ±0.5°, respectively. The accuracy is improved to 0.1° by combining mechanical alignment and LEDBH$_2$ detection using YOLOv7. Figure 10(b) shows throughputs after fine adjustment of the offset angle, θ_1, to 0° within a range of ±1.2°. LEDBH$_1$ can be accurately aligned to 0° using the LEDBH$_2$ detection image. The variations in throughput were suppressed to a maximum of 7 Mbps for Tx and 0.1 Mbps for Rx. The object detection within $\theta_1 = \pm1.2°$ was demonstrated.

Figure 11 shows examples of LEDBH$_2$ detection within
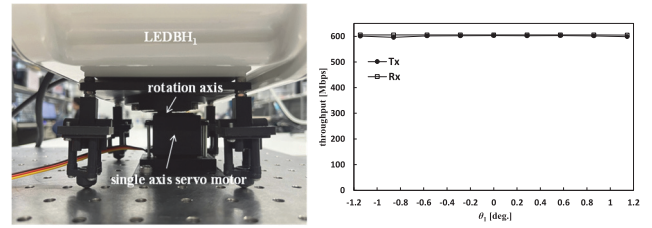
(a) single-axis control mechanism   (b) throughputs after fine adjustment

Fig. 10 Control mechanism and throughput after fine adjustment, where the exposure time is further reduced to 34μs ($\theta_2 = 0°$, $d = 10$ m).
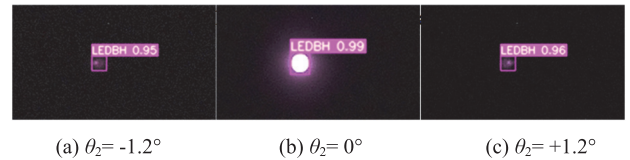

(a) θ_2= -1.2°   (b) θ_2= 0°   (c) θ_2= +1.2°

Fig. 11 Examples of LEDBH$_2$ detection within $\theta_2 = \pm1.2°$, where $\theta_1 = 0°$.

$\theta_2 = \pm1.2°$, where $\theta_1 = 0°$. Although the peak of the detected image shifts to the left at $\theta_2 = -1.2°$, to the center at 0°, and to the left at +1.2°, confidence scores of more than 0.95 are obtained. The object detection within $\theta_2 = \pm1.2°$ was demonstrated.

5. Conclusion

High-precision automatic optical axis alignment of 600 Mbps near-IR LEDBH was achieved by object detection using YOLOv7. APs of LEDBH detection are evaluated in lighting surroundings while changing the exposure time of VL camera without IR cut filter. The object detection using short-exposure-time camera can learn the differences in radiation pattern between LEDBH and other LED lighting. High-throughput 600 Mbps transmission was maintained with an accuracy of 0.1° by aligning the optical axis based on object detection within $\theta_1 = \pm1.2°$.

References

[1] H. Haas, L. Yin, C. Chen, S. Videv, D. Parol, E. Poves, H. Alshaer, and M.S. Islim, "Introduction to indoor networking concepts and challenges in LiFi," *Journal of Optical Communications and Networking*, vol. 12, no. 2, pp. 190–203, Feb. 2020. DOI: 10.1364/JOCN.12.00A190

[2] T. Cogalan, D. Camps-Mur, J. Gutiérrez, S. Videv, V. Sark, J. Prados-Garzon, J. Ordonez-Lucena, H. Khalili, F. Cañellas, A. Fernández-Fernández, M. Goodarzi, A. Yesilkaya, R. Bian, S. Raju, M. Ghoraishi, H. Haas, O. Adamuz-Hinojosa, A. Garcia, C. Colman-Meixner, A. Mourad, and E. Aumayr, "5G-CLARITY: 5G-advanced private networks integrating 5GNR, WiFi, and LiFi," *IEEE Commun. Mag.*, vol. 60, no. 2, pp. 73–79, Feb. 2022. DOI: 10.1109/MCOM.001.2100615

[3] D. Schulz, V. Jungnickel, C. Alexakis, M. Schlosser, J. Hilt, A. Paraskevopoulos, L. Grobe, P. Farkas, and R. Freund, "Robust optical wireless link for the backhaul and fronthaul of small radio cells,"

J. Lightw. Technol., vol. 34, no. 6, pp. 1523–1532, March 2016. DOI: 10.1109/JLT.2016.2523801

[4] A. Gomez, K. Shi, C. Quintana, G. Faulkner, B.C. Thomsen, and D. O'Brien, "A 50 Gb/s transparent indoor optical wireless communications link with an integrated localization and tracking system," *J. Lightw. Technol.*, vol. 34, no. 10, pp. 2510–2517, May 2016. DOI: 10.1109/JLT.2016.2542158

[5] B. Fahs, M. Romanowicz, J. Kim, and M.M. Hella, "A self-alignment system for LOS optical wireless communication links," *IEEE Phtonics Technol. Lett.*, vol. 29, no. 24, pp. 2207–2210, Dec. 2017. DOI: 10.1109/LPT.2017.2771303

[6] M.R. Rahman, T.V. Sethuraman, M. Gruteser, K.J. Dana, S. Jain, N.B. Mandayam, and A. Ashok, "Camera-based light emitter localization using correlation of optical pilot sequences," *IEEE Access*, vol. 10, pp. 24368–24382, Feb. 2022. DOI: 10.1109/ACCESS.2022.3153708

[7] M.A. Arfaoui, M.D. Soltani, I. Tavakkolnia, A. Ghrayeb, C. Assi, M. Safari, and H. Haas, "Invoking deep learning for joint estimation of indoor LiFi user position and orientation," *IEEE J. Sel. Areas Commun.*, vol. 39, no. 9, pp. 2890–2905, Sept. 2021. DOI: 10.1109/JSAC.2021.3064637

[8] I.B.K.Y. Utama, M.H. Rahman, B. Chung, and Y.M. Jang, "Intelligent receiver for optical camera communication," 2022 International Conference on Artificial Intelligence in Information and Communication, pp. 96–100, Feb. 2022. DOI: 10.1109/ICAIIC54071.2022.9722631